Journal of Engineering and Applied Sciences 13 (23): 9831-9837, 2018
ISSN: 1816-949X

The Effect of pH Values of ZnS Nanoparticles on Photoelectrode Performance of Flexible Dye Sensitized Solar Cell

[1]Ghaida. Salman, [1]Manal Medhat and [2]Abdulkareem Mohammed Ali Al-Sammarraie
[1]Department of Physics,
[2]Department of Chemistry, College of Science, Baghdad University, Baghdad, Iraq

Abstract: A flexible DSSC with dimension (2×2.5) cm is fabricated and characterized. Titania nanotube arrays /ZnS nanoparticles (TNT/ZnS NPs) are assembled by the deposition of ZnS nanoparticles onto the anodized TiO_2 nanotube arrays via sequent-chemical bath deposition. Prior to solar cell construction, the tube-based photo-anodes are annealed at temperature (550°C) and for 2 h. The effect of pH value (7.5, 8.5 and 9.5) of prepared ZnS NPs on the photovoltaic performance of the solar cells is investigated. The performance of the flexible DSSCs was studied in detail using a ployaniline counter electrode and KI/I3 electrolyte. Ruthenium (Ru) dye (N719) was used as an active layer. Characterizations of the films were performed by using scanning electron microscopy, energy dispersive X-ray spectroscopy, X-ray diffractometry. The optimized device performanc of the TNT/ZnS NPs photoanode of ZnS pH value equal to (8.5) displayed the highest conversion efficiency of 1.09% which is higher than that of the other photoelectrodes. The fabricated device showed JSC, VOC and FF values of (4 mA cm^{-2}, 0.39 V and 0.55), respectively.

Key words: Flexible DSSCs, TiO_2 nanotube, composite material, anodization, photoanode, sensitizer, photovoltaic

INTRODUCTION

Recent progress in plastic electronics obtained at low temperature attracts technologies of printable materials to develop thin and cost-effective devices. Dye-Sensitized Solar Cell (DSSC) is one among them, due to its low cost, easy production and acceptable efficiency when compared to conventional silicon solar cells (Lee *et al*., 2014). DSSCs kept the attention of the technological and scientific community for their promising additional properties such as the flexibility and low fabrication costs. They are considered as third generation photovoltaic cells (Faccio *et al*., 2011). DSSCs are composed of four parts as follows: the electrode film layer (TiO_2), covered by a monolayer of dye molecules, that absorbs solar energy, the conductive transparent oxide layer that facilitates charge transfer from the electrode layer, the counter electrode layer made of such as Pt or C, the redox electrolyte layer for reducing the level of energy supplied from the dye molecules. Research efforts to improve the efficiency of DSSCs have primarily been focused on improvements of the each DSSC component (Yang *et al*., 2014).

Anatase TiO_2 is core inorganic material that is capable of efficiently harvesting light and is considered the prominent cathode electrode material in solar cells. Among different shapes of titania, TiO_2 nanotubes have raised a lot of interest in the last decades (Kim *et al*., 2006). In a DSSC, the photo-excited electrons of the dye molecules are transferred to the TiO_2 conduction band which are taken out through an external circuit using an anode electrode (fluorine-doped tin oxide or indium-doped tin oxide) and a counter electrode (platinum or carbon sputtered FTO), respectively, in the presence of a liquid or solid redox electrolyte (Yan and Zhou, 2011).

In recent years, encouraging conversion efficiency of liquid electrolyte DSSCs has been achieved by optimized counter-electrodes, new routes of sensitization and surface passivation such as depositing a thin layer (insulating metal oxides (Al_2O_3), ZnS or SiO_2) on the surface of ZnO or TiO_2. One of the most widely used techniques is the deposition of a ZnS layer on the surface of TiO_2 photoanode taking advantage of the easy preparation and the striking enhancement of the efficiency achieved. ZnS is constituted by more earth-abundant elements and depositing ZnS layer between the TiO_2 and dye molecules is useful to enhance the electron injection and reduce the charge recombination (Rezvani *et al*., 2016).

The DSSCs fabrication can be switched from traditional glass substrates to either flexible plastic or metal and can be fabricated in different combination. By fabricating of DSSCs on light weight and flexible substrates and also, implementing roll-to-roll processing, large cost reductions could be expected even be halved compared to glass based batch process DSSCs technology (Yugis *et al*., 2015). In this study in order to fabricate a flexible DSSC (2×2.5) cm a composite material

Corresponding Author: Ghaida Salman, Department of Physics, College of Science, Baghdad University, Baghdad, Iraq

of TiO_2 Nanotube/ZnS Nanoparticle (TNT/ZnS NPs) were assembled by the deposition of ZnS nanoparticles onto the anodized TiO_2 nanotube layer via sequent-chemical bath deposition technique.

MATERIALS AND METHODS

To prepare the TiO_2 nanotube photoanode using anodization method, Ti foil substrate was first cleaned with Deionized (DI) water, then with ethanol and acetone for 10 min for each using an ultrasonic bath. Anodic oxidation of Ti foil is performed in a two-electrode cell with Ti foil acting as the working electrode while a Pt as the counter electrode and 0.5 wt.% NH_4F dissolved in 50 mL anhydrous ethylene glycol with 4 vol% water solution as the electrolyte at 30 V for 2 h. Then, the samples are rinsed in ethanol and dried by a heated air gun. Then, after many experiments to obtain the optimum annealing temperature, the samples annealed at 5°C for 2 h.

The deposition of ZnS nanoparticles onto the annealed TiO_2 nanotube arrays was performed by sequent-CBD method. The zinc sulfide ZnS nanoparticles were prepared by two chemical solutions of 0.1M: the first one is prepared by dissolving 1.36 g of zinc chloride powder $ZnCl_2$ in 100 mL distilled water. Ammonia was added to the mixture to adjust the pH of the solution to the required levels of (pH = 7.5, 8.5 and 9.5). While the second solution is obtained by dissolving 0.78 g from sodium sulfide powder Na_2S in 100 mL distilled water. The TNT sample is immersed in the cationic precursor for 3 min. where adsorption of Zn+ ions takes place on the surface of TNT and the unadsorbed ions were removed by rinsing the TNT in DI water for 10 sec. Then, this sample is immersed in an anionic precursor for 3 min, S^- ions are reacted with Zn+ ions. The loosely bound ions were removed by rinsing the sample in the deionized water for 10 sec. Thus, one layer of ZnS is formed, this completes one sequent-CMD cycle. These sequent CBD cycles were repeated 5 times until the required film thickness was reached (Shinde *et al*., 2011). The schematic diagram of the fabricated device is presented in Fig. 1.

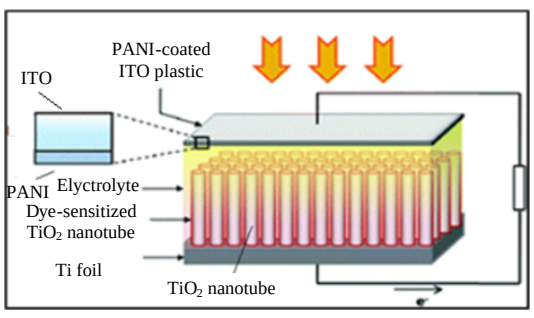

Fig. 1: A schematic diagram of the assembled flexible DSSC

The crystal structure of the prepared materials is examined by using X-Ray Diffraction (XRD). The surface features and morphology of the photoanodes were determined by using a Field Emission Scanning Electron Microscope (FE-SEM, S-4200 and Hitachi) operated at 15 kV. The elemental composition of ZnS was identified by energy-dispersive X-Ray Spectroscopy (EDX). The photocurrent density-voltage (I-V) characteristics of the assembled flexible DSSCs were found using a solar simulator (80 mW cm^{-2} am 1.5) illumination.

RESULTS AND DISCUSSION

Structural studies of the electropolymerized polyaniline on ITO plastic counter electrode

X-ray diffraction study: The crystal structure of the deposited PANI on ITO plastic substrate was examined by X-Ray Diffraction (XRD) patterns as shown in Fig. 2. In the XRD pattern of PANI, the characteristic peaks appearing at 2θ of 9.49, 19.28, 25.7 and 29.2° which correspond to the (001), (020) and (200) and (022) crystal planes of PANI. This result is comparable with result of other researchers (Devi *et al*., 2014).

FTIR spectrum study: The Fourier Transformation Infrared spectra (FTIR) of electropolymerized PANI is investigated as shown in Fig. 3. In the spectrum the band observed at 3429.2 cm^{-1} is due to O-H stretching vibrations. The polymer shows the absorption band at 2879.52 cm^{-1} is due to symmetric C-H stretching vibrations (Devi *et al*., 2014). The peaks at 1564.16 cm^{-1} and 1488.94 cm^{-1} are attributed to the C = C stretching of quinonoid rings and C = C stretching of benzenoid rings, respectively (Mandal *et al*., 2014). The characteristic peak at 1236.29 cm^{-1} and 1299.93 are due to C-N stretching of primary aromatic amines (Devi *et al*., 2014; Vivekanandan *et al*., 2011).

Absorption spectrum for ruthenium-N719 dye: The electric current generation by harvesting the solar irradiation and injecting the excited electrons into the TiO_2

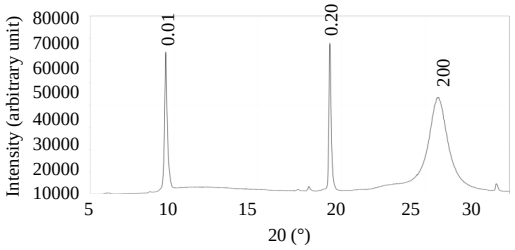

Fig. 2: XRD spectrum of electropolymerized PANI

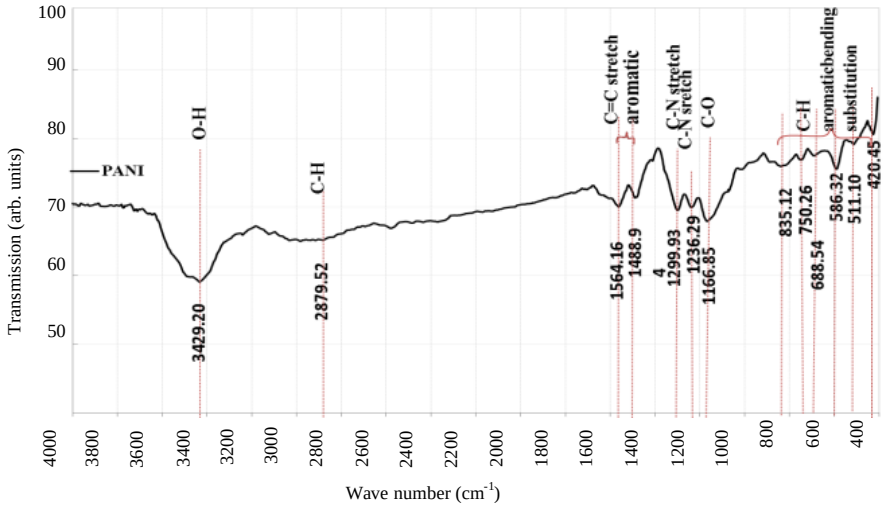

Fig. 3: Infrared spectra of electropolymerized PANI

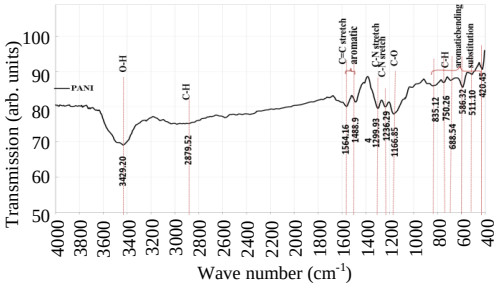

Fig. 4: Absorbance spectrum of N719 dye as function of wavelength

conduction band in DSSCs is only done by the sensitizer which plays the crucial role (Rao *et al*., 2015). Ru-N719 dye solution was prepared by adding 3.56 mg of Ru-N719 to 10 mL of ethanol. The absorption spectrum (300-700) of the dye that was adsorbed from pure TiO_2 films and composite films was measured by UV-Vis spectroscopy as shown in Fig. 4. Two main peaks were observed at 384 nm and 527 nm. This result is comparable with result obtained by Arifin *et al*. (2017).

Structural properties of TiO$_2$ nanotubes (TNT) prepared by anodizing process

X-ray diffraction results: X-ray diffraction pattern of Titania Nanotube (TNT) and TNT/ZnS NPs photoanode for anodization time of 2 h on Ti foil substrate with annealing of TNT layer at temperature 550°C is shown in Fig. 5.

It was found that the TiO_2 nanotubes grown on Ti substrates have an anatase structure (JCPDS: 96-900-9087). Three diffraction peaks were observed at around 25, 37.7 and 53.9° which are corresponding to (101), (004) and (105) crystal planes, respectively. Meanwhile, the ZnS NPs/TNT films with different pH values for ZnS NPs exhibit weak diffraction peaks at 2$_e$° = 27.3, 31.4 and 47.8 corresponding to the (100), (101) and (110) hexagonal form of ZnZ NPs (JCPDS: 96-901-3421).

Due to the annealing at high temperature of 550°C of TNT films, the diffraction peaks become sharp and the Full Width at Half Maximum (FWHM) is narrow. These results were used to calculate the crystallite size by using the Debye-Scherrer's equation. The diffraction peaks of TNT at 2$_e$° = 25° and ZnS at 2$_e$° = 27.3° were used as the reference peak. The calculated crystallite size value of TNT was 23.7 nm while the obtained crystallite size of the ZnS NPs/TNT with different values of pH for ZnS NPs was 30 nm. Table 1 shows the X-ray diffraction pattern parameters for flexible DSSC photoanodes.

Scanning Electron Microscope (SEM) analysis: The deposition of ZnS nanoparticles on the TNT surface is necessary to obtain a high specific surface area and adhesion between the film and substrate. Fig. 6 illustrates the SEM images of the bare TNT and TNT/ZnS NPs electrodes on Ti foil substrate and for pH of ZnS NPs equal to 8.5.

Figure 6a shows the self-organized TNT produced on Ti foil via electrochemical anodization at 30 V and for 2 h. The diameters of the obtained TiO_2 nanotubes are in the range of (96) nm.

In comparison with the bare TNT film as shown in Fig. 6b, uniform distribution of the as-deposited ZnS NPs was formed on the surface of TiO_2 nanotubes. However, there is a good embedding of ZnS NPs on the

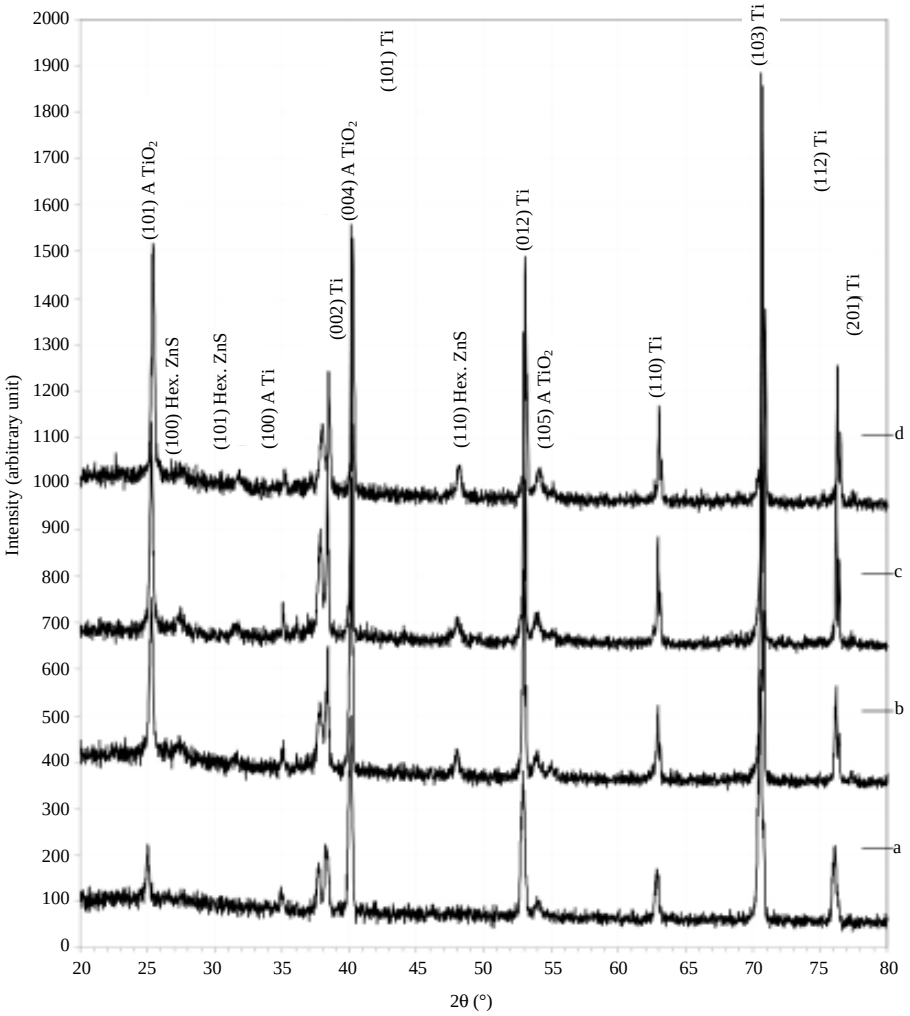

Fig. 5: XRD patterns for flexible DSSC photoanodes for anodization time 2 h and (after annealing): a) TiO_2 nanotubes; b) ZnS NPs/TNT (pH = 7.5); c) ZnS NPs/TNT (pH = 8.5) and d) ZnS NPs/TNT(pH = 9.5)

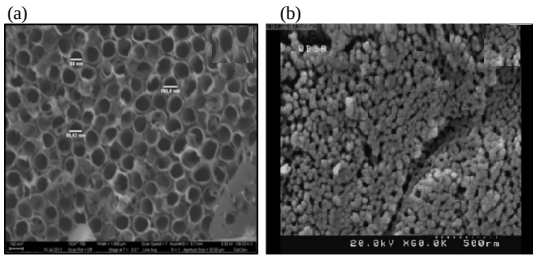

Fig. 6: SEM images of the films of: a) Bare TiO_2 nanotubes and b) TNT/ZnS NPs photoanode

TNT nanotubes arrays. As seen in this figure, there are number of large size of ZnS NPs at the mouth of the TNT. However, the annealing temperature at 550°C of TNT has resulted in the blockage of the mouth of the nanotubes before the deposition of ZnS NPs.

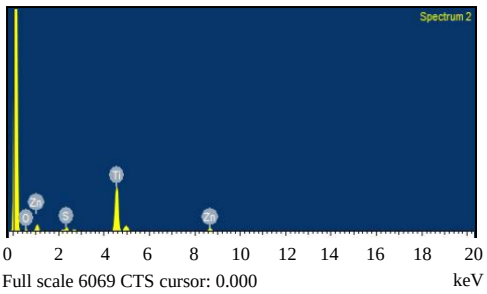

Fig. 7: EDX spectrum of the: a) TiO_2 nanotube and b) TNT/ZnS photoanode respectively

Composition Analysis: Energy-Dispersive X-ray spectroscopy (EDX) analysis was used to identify the elemental compositions of the prepared electrodes on the Ti foil substrates. Figure 7 shows the representative EDX

Table 1: X-ray diffraction pattern parameters for flexible DSSC photoanodes

pH	2θ (deg.)	FWHM (deg.)	d_{hkl}exp. (Å)	GS (nm)	hkl	d_{hkl}Std. (Å)	Phase	Card No.
TiO_2 bare	25.057	0.3437	3.5510	23.7	(101)	3.5169	Anatase	96-900-9087
	34.877	0.3436	2.5704	24.2	(100)	2.5525	Ti	96-900-8518
	37.765	0.2946	2.3802	28.5	(004)	2.3785	Anatase	96-900-9087
	38.216	0.3928	2.3531	21.4	(002)	2.3411	Ti	96-900-8518
	40.131	0.3437	2.2452	24.6	(101)	2.2415	Ti	96-900-8518
	52.946	0.3928	1.7280	22.6	(012)	1.7255	Ti	96-900-8518
	53.928	0.4419	1.6988	20.2	(105)	1.7001	Anatase	96-900-9087
	62.864	0.3437	1.4771	27.1	(110)	1.4738	Ti	96-900-8518
	70.622	0.5401	1.3327	18.0	(103)	1.3316	Ti	96-900-8518
	76.072	0.3928	1.2502	25.7	(112)	1.2473	Ti	96-900-8518
	77.201	0.3928	1.2347	25.9	(201)	1.2313	Ti	96-900-8518
7.5	25.254	0.3437	3.5238	23.7	(101)	3.5169	Anatase	96-900-9087
	27.365	0.5892	3.2565	13.9	(100)	3.2710	Hex ZnS	96-901-3421
	31.489	0.5892	2.8388	14.0	(101)	2.8918	Hex ZnS	96-901-3421
	35.074	0.2454	2.5564	34.0	(100)	2.5525	Ti	96-900-8518
	37.823	0.3437	2.3767	24.4	(004)	2.3785	Anatase	96-900-9087
	38.412	0.1964	2.3416	42.8	(002)	2.3411	Ti	96-900-8518
	40.131	0.3928	2.2452	21.5	(101)	2.2415	Ti	96-900-8518
	47.987	0.3928	1.8943	22.1	(110)	1.8885	Hex ZnS	96-901-3421
	52.995	0.1964	1.7265	45.2	(012)	1.7255	Ti	96-900-8518
	53.928	0.3928	1.6988	22.7	(105)	1.7001	Anatase	96-900-9087
	62.962	0.2455	1.4751	37.9	(110)	1.4738	Ti	96-900-8518
	70.622	0.3928	1.3327	24.8	(103)	1.3316	Ti	96-900-8518
	76.219	0.2946	1.2481	34.3	(112)	1.2473	Ti	96-900-8518
	77.349	0.3437	1.2327	29.6	(201)	1.2313	Ti	96-900-8518
8.5	25.254	0.2455	3.5238	33.2	(101)	3.5169	Anatase	96-900-9087
	27.414	0.5401	3.2508	15.1	(100)	3.2710	Hex ZnS	96-901-3421
	31.637	0.7365	2.8259	11.2	(101)	2.8918	Hex ZnS	96-901-3421
	35.074	0.1963	2.5564	42.4	(100)	2.5525	Ti	96-900-8518
	37.823	0.2946	2.3767	28.5	(004)	2.3785	Anatase	96-900-9087
	38.314	0.1964	2.3473	42.8	(002)	2.3411	Ti	96-900-8518
	40.180	0.2455	2.2425	34.5	(101)	2.2415	Ti	96-900-8518
	47.938	0.5892	1.8962	14.8	(110)	1.8885	Hex ZnS	96-901-3421
	52.995	0.2455	1.7265	36.2	(012)	1.7255	Ti	96-900-8518
	53.928	0.4419	1.6988	20.2	(105)	1.7001	Anatase	96-900-9087
	62.962	0.2946	1.4751	31.6	(110)	1.4738	Ti	96-900-8518
	70.769	0.3928	1.3303	24.8	(103)	1.3316	Ti	96-900-8518
	76.219	0.2455	1.2481	41.1	(112)	1.2473	Ti	96-900-8518
	77.398	0.3928	1.2320	25.9	(201)	1.2313	Ti	96-900-8518
9.5	25.401	0.2455	3.5037	33.2	(101)	3.5169	Anatase	96-900-9087
	27.561	0.5401	3.2338	15.1	(100)	3.2710	Hex ZnS	96-901-3421
	31.784	0.6383	2.8131	12.9	(101)	2.8918	Hex ZnS	96-901-3421
	35.172	0.2946	2.5495	28.3	(100)	2.5525	Ti	96-900-8518
	38.020	0.3437	2.3648	24.4	(004)	2.3785	Anatase	96-900-9087
	38.511	0.1964	2.3358	42.8	(002)	2.3411	Ti	96-900-8518
	40.229	0.2455	2.2399	34.5	(101)	2.2415	Ti	96-900-8518
	48.232	0.4419	1.8853	19.7	(110)	1.8885	Hex ZnS	96-901-3421
	53.093	0.3437	1.7236	25.8	(012)	1.7255	Ti	96-900-8518
	54.075	0.4910	1.6945	18.2	(105)	1.7001	Anatase	96-900-9087
	63.061	0.2946	1.4730	31.6	(110)	1.4738	Ti	96-900-8518
	70.671	0.2455	1.3319	39.7	(103)	1.3316	Ti	96-900-8518
	76.318	0.2946	1.2468	34.3	(112)	1.2473	Ti	96-900-8518
	77.447	0.2455	1.2314	41.5	(201)	1.2313	Ti	96-900-8518

Table 2: The composition of TNT/ ZnS NPs photoanode determined by EDX

Element	Weight (%)	Atomic (%)
O K	26.570	52.96
S K	2.1700	2.150
Ti K	56.900	37.88
Zn K	14.360	7.010
Totals	100.00	

pattern of Ti, O, Zn and S elements which confirms the formation TNT/ ZnS photoanode. This means that the film quality is good, since, there is no presence of other compounds observed. Main conclusions can be obtained from data which were listed in Table 2.

J-V characterization of assembled flexible DSSCs for 2 h anodization time and annealed TNT layer: Figure 8 shows the J-V characteristics curves under an illumination of 80 mW/cm^2 conditions at room temperature of all the assembled flexible DSSCs of bare TNT photoanode and

Table 3: Parameters of the assembled flexible DSSCs from PANI/ ITO plastic sheet as catalyzed cathodes and different photoanodes

Cathode	Photoanode	pH value of ZnS NPs	JSC (mA)	VOC (V)	Im (mA)	Vm (V)	FF	η (%)
PANI/ITO plastic	TNT (bare)	¾	1.640	0.350	1.100	0.300	0.575	0.300
PANI/ITO plastic	TNT/ZnS NPs	7.5	0.240	0.154	0.150	0.120	0.487	0.330
PANI/ITO plastic	TNT/ZnS NPs	8.5	4.000	0.390	2.600	0.335	0.558	1.089
PANI/ITO plastic	TNT/ZnS NPs	9.5	4.100	0.390	2.200	0.320	0.440	0.880

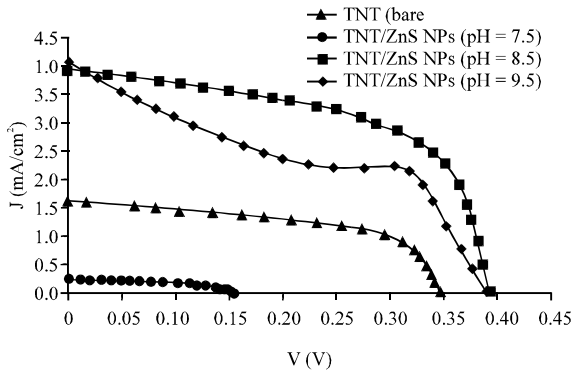

Fig. 8: J-V characteristics of the assembled flexible DSSCs from PANI/ ITO plastic sheet as catalyzed cathodes and different photoanodes, for anodization time 2 h and (with annealing)

TNT/ZnS NPs with different pH values photoanodes. The anodization time of TNT is 2 h and before the deposition of ZnS NPs layer, the TNT film was annealed at temperature of 550°C for 2 h. This figure explains the effect of photoanode materials on the performance of the assembled flexible DSSCs. The values of solar cell parameters are listed in Table 3.

It is obvious from Fig. 8, that using of bare (TNT) as a photoelectrode and PANI/ITO plastic as counter electrode, the fabricated cell exhibited Jsc and VOC and FF values of (1.64 mA cm^{-2}, 0.35 V and 0.57), respectively, resulting in a low efficiency of 0.3%.

The optimized device performanc of the TNT/ZnS NPs of ZnS (pH value of ZnS equal to 8.5 electrode displayed the highest conversion efficiency of 1.09% among other pH values. The fabricated device shows Jsc, Voc and FF values of (4 mA cm^{-2}, 0.39 V and 0.55), respectively. It can be concluded that the enhanced power conversion efficiency mostly arises from the positive influence of ZnS on TNT which resulted in enhanced photo-electron harvesting efficiency of the photoanode and relatively low resistivity. However, ZnS deposited on the TNT surface or combination of TNT/ZnS NPs shows appreciably better photocatalytic activity than the bare TiO_2 nanotube film. Moreover, deposition of the ZnS layer on TiO_2 nanotube influences the light absorbance properties and the electron transport (Rao *et al.*, 2015).

Also, the performance of the TNT/ZnS NPs of ZnS pH values equal to 7.5 and 9.5 photoelectodes (, = 0.33%, JSC = 0.24 mA cm^{-2}, Voc = 0.15 V and FF = 0.48) and (, = 0.88%, JSC = 4.1 $mAcm^{-2}$, VOC = 0.39 V and FF = 0.44), respectively. The decrease in JSC for the TNT/ZnS NPs of ZnS pH values equal to 7.5 and 9.5 photoelectodes, resulting from its lower conductivity and catalytic activity for the I_3-reduction. However, the effect of ZnS pH values on TNT will change the optical band gap and the insulating properties of TNT films which drastically reduces the rate of electron transfer from the photoanode to Ti foil and then to the external circuit.

CONCLUSION

In summary, TNT/ZnS NPs photoanodes were successfully prepared via two deposition methods: TiO_2 nanotubes are first grown on Ti foil substrate by using anodization method followed by coating of ZnS NPs on the TNT layer by sequent CBD method. We have demonstrated that ZnS NPs deposited on the surface of TiO_2 nanotube films can be used as photoanodes in flexible DSSCs. The optimized device result is obtained for the photoelectrode of ZnS pH value equal to (8.5) in conjunction with the KI/I_2 electrolyte and PANI on ITO plastic as a counter electrode. Under illumination of simulated (80 mW cm^{-2}), the optimized device exhibited the highest conversion efficiency of 1.089% which is higher than that of the other photoelectrodes. The fabricated device showed JSC, VOC and FF values of (4 mA cm^{-2}, 0.39 V and 0.55), respectively.

SUGGESTIONS

This suggests that the promising ZnS NPs-coated TiO_2 nanotubes collect a large number of photo-injected electrons in the conduction band of the photoanode and the N719 dye reduce the recombination of photo-injected electrons with the redox electrolyte. Thermal annealing of TNT layer at temperature 550°C and for 2 h. was applied to enhance the photoelectrochemical properties of the TNT/ZnS NPs photoanodes.

REFERENCES

Arifin, Z., S. Soeparman, D. Widhiyanuriyawan and S. Suyitno, 2017. Performance enhancement of dye-sensitized solar cells using a natural sensitizer. Intl. J. Photoenergy, 2017: 1-5.

Devi, M.R., B. Lawrence, N. Prithivikumaran and N. Jeyakumaran, 2014. Synthesis and characterization of conducting polymer polyaniline doped with salicylic acid. Chem. Tech. Res., 6: 5400-5403.

Faccio, R., L.F. Andez-Werner, H. Pardo and W.A. Mombru, 2011. Current trends in materials for dye sensitized solar cells. Recent Patents Nanotechnol., 5: 46-61.

Kim, S.S., Y.C. Nah, Y.Y. Noh, J. Jo and D.Y. Kim, 2006. Electrodeposited Pt for cost-efficient and flexible dye-sensitized solar cells. Electrochim. Acta, 51: 3814-3819.

Lee, K.M., L.C. Lin, C.Y. Chen, V. Suryanarayanan and C.G. Wu, 2014. Preparation of high transmittance platinum counter electrode at an ambient temperature for flexible dye-sensitized solar cells. Electrochim. Acta, 135: 578-584.

Mandal, M., D. Ghosh, S. Giri, I. Shakir and C.K. Das, 2014. Polyaniline-wrapped 1D $CoMoO_4.0.75H_2O$ nanorods as electrode materials for supercapacitor energy storage applications. RSC. Adv., 4: 30832-30839.

Rao, S.S., D. Punnoose, C.V. Tulasivarma, C.P. Kumar and C.V. Gopi *et al*., 2015. A strategy to enhance the efficiency of dye-sensitized solar cells by the highly efficient TiO 2/ZnS photoanode. Dalton Trans., 44: 2447-2455.

Rezvani, F., E. Parvazian and S.A. Hosseini, 2016. Dye-sensitized solar cells based on composite TiO_2 nanoparticle-nanorod single and bi-layer photoelectrodes. Bull. Mater. Sci., 39: 1397-1402.

Shinde, M.S., P.B. Ahirrao, I.J. Patil and R.S. Patil, 2011. Studies on nanocrystalline ZnS thin films prepared by modified chemical bath deposition method. Indian J. Pure Appl. Phys., 49: 765-768.

Vivekanandan, J., V. Ponnusamy, A. Mahudeswaran and P.S. Vijayanand, 2011. Synthesis, characterization and conductivity study of polyaniline prepared by chemical oxidative and electrochemical methods. Arch. Appl. Sci. Res., 3: 147-153.

Yan, J. and F. Zhou, 2011. TiO_2 nanotubes: Structure optimization for solar cells. J. Mater. Chem., 21: 9406-9418.

Yang, J.H., C.W. Bark, K.H. Kim and H.W. Choi, 2014. Characteristics of the dye-sensitized solar cells using TiO_2 nanotubes treated with $TiCl_4$. Mater., 7: 3522-3532.

Yugis, A.R., R.F. Mansa and C.S. Sipaut, 2015. Review on metallic and plastic flexible dye sensitized solar cell. Mater. Sci. Eng., 78: 1-7.November 19, 2018